Including nuclear quantum effects into highly correlated electronic structure calculations of weakly bound systems

Néstor F. Aguirre, Pablo Villarreal, Gerardo Delgado-Barrio, Edwin Posada, Andrés Reyes et al.

Citation: J. Chem. Phys. **138**, 184113 (2013); doi: 10.1063/1.4803546
View online: http://dx.doi.org/10.1063/1.4803546
View Table of Contents: http://jcp.aip.org/resource/1/JCPSA6/v138/i18
Published by the American Institute of Physics.

Including nuclear quantum effects into highly correlated electronic structure calculations of weakly bound systems

Néstor F. Aguirre,[1] Pablo Villarreal,[1] Gerardo Delgado-Barrio,[1] Edwin Posada,[2] Andrés Reyes,[2] Malgorzata Biczysko,[3] Alexander O. Mitrushchenkov,[4] and María Pilar de Lara-Castells[1,a)]

[1]*Instituto de Física Fundamental (C.S.I.C.), Serrano 123, E-28006 Madrid, Spain*
[2]*Departamento de Química, Universidad Nacional de Colombia, Av. Cra. #45-03 Bogotá, Colombia*
[3]*Center for Nanotechnology Innovation @NEST, Istituto Italiano di Tecnologia, Piazza San Silvestro 12, I-56127 Pisa, Italy and Scuola Normale Superiore, Piazza dei Cavalieri 7, I-56126 Pisa, Italy*
[4]*Université Paris-Est, Laboratoire Modélisation et Simulation Multi Echelle, MSME UMR 8208 CNRS, 5 bd Descartes, 77454 Marne-la-Vallée, France*

(Received 23 February 2013; accepted 17 April 2013; published online 14 May 2013)

An interface between the APMO code and the electronic structure package MOLPRO is presented. The any particle molecular orbital APMO code [González *et al.*, Int. J. Quantum Chem. **108**, 1742 (2008)] implements the model where electrons and light nuclei are treated simultaneously at Hartree-Fock or second-order Möller-Plesset levels of theory. The APMO-MOLPRO interface allows to include high-level electronic correlation as implemented in the MOLPRO package and to describe nuclear quantum effects at Hartree-Fock level of theory with the APMO code. Different model systems illustrate the implementation: $^4He_2$ dimer as a protype of a weakly bound van der Waals system; isotopomers of $[He–H–He]^+$ molecule as an example of a hydrogen bonded system; and molecular hydrogen to compare with very accurate non-Born-Oppenheimer calculations. The possible improvements and future developments are outlined. © *2013 AIP Publishing LLC*. [http://dx.doi.org/10.1063/1.4803546]

I. INTRODUCTION

It is well known that nuclear quantum effects play a significant role in a wide variety of relevant systems implying light nuclei such as hydrogen-bonded systems and helium droplets. In fact, spectroscopic probes of molecular impurities in helium droplets have shown that while ^{4}He clusters result in superfluid behavior with free-rotor-like molecular spectra, ^{3}He atoms behave as a normal fluid and the impurity spectra are of hindered-rotor type.[1] Since ^{4}He atoms are composite spinless bosons and ^{3}He atoms are fermionic particles with a nuclear spin equal to 1/2, one fundamental question has concerned the influence of the spin and the antisymmetry of the fermionic ^{3}He wave-functions in providing such different response to the molecular rotation. Quantum-Chemistry (QC)-like Nuclear-Orbital (NO) approaches, first introduced by Jungwirth and Krylov,[2] map the problem onto an electronic structure-like problem by considering the helium atoms as *pseudo-electrons* and the dopant molecule as a structured pseudo-nucleus, replacing Coulomb interactions by van der Waals He–He and He-dopant pair potentials. This way, the dopant molecule is considered as fixed, assuming the Born-Oppenheimer (BO) separation between the nuclear motions of the helium atoms and the dopant, and an expansion over Gaussian-type functions (GTFs) centered on the dopant can be employed.[2] Later, this QC-like NO approach was reformulated in internal coordinates by separating the center-of-mass operator from the Hamiltonian and employing radial basis functions centered on the dopant-He internuclear distance, in contrast with standard electronic structure problems. Within this framework, multi-orbital Hartree and Hartree-Fock (HF) implementations were developed.[3,4] Hereafter, the Full-Configuration-Interaction (FCI) NO approach was designed to deal with ^{3}He atoms[5,6] and extended to bosonic ^{4}He atoms and *para*-H_2 molecules.[7] The essential merit of these QC-like approaches consists in using nuclear orbitals to describe one-particle helium states so that bosonic/fermionic symmetry can be easily included[3,5–8] on an equal footing, allowing a natural extension of theoretical concepts that have served molecular structure theory. These approaches rely on the BO approximation so that the nuclear quantum effects (NQE) are introduced after performing the standard clamped-nuclei electronic structure calculations that provide the potential energy surface on which the nuclear motion occurs.

A number of theoretical approaches for NQE that have been developed, are mainly aimed to describe systems involving hydrogen-bonding, hydrogen transfer processes, and small hydrogen-containing molecules beyond the BO approximation. Some of these methods use a one-particle molecular orbital picture for both electrons and the lightest nuclei (e.g., proton, deuteron, etc.), achieving a simultaneous instead of sequential quantum-mechanical description of these particles. The underlying idea was put forward in the late 1960s by Thomas and collaborators[9–12] and applied to methane, ammonia, and water, using Slater orbitals for the protons (SNO). A few years later, Bishop and collaborators[13,14] studied H_2^+ and isotopologues with an accurate non-adiabatic variational approach. It also worths mentioning the molecular coupled-

a)Author to whom correspondence should be addressed. Electronic mail: Pilar.deLara.Castells@csic.es

cluster (MCC) method formulated by Monkhorst in the late 1980s,[15] in which the electrons and nuclei are described simultaneously with the coupled-cluster (CC) approach.

Over the last years, a renewed interest in nuclear-electron orbital approaches has been raised in order to analyze, for instance, isotope effects and hydrogen tunneling. One of their attractive features is the capability of incorporating finite nuclear mass/isotope and spin statistic effects directly into the electronic wave-function, in a contrast with BO treatments where these finite-mass effects are usually incorporated as corrections, either adiabatic or non-adiabatic, to the electronic energies only (see, e.g., Ref. 16). In fact, approaches going beyond the BO approximation and enabling a simultaneous description of electrons and nuclei are very useful when the nuclear de-localization has a marked influence onto the electronic wave-function itself (e.g., proton-coupled electron transfer processes). The most rigorous non-BO methods are aimed to solve the all-particle Schrödinger equation of small atomic and molecular systems as accurately as possible, taking into account the translational and rotational invariance of the molecular Hamiltonian. Within this framework, the methodological contributions from Adamowicz and collaborators[17–19] have the longest history (for a very recent review, see Ref. 19). Starting with the separation of the center-of-mass operator from the molecular Hamiltonian, one key characteristic of these methodological developments is the employment of explicitly correlated Gaussian (ECG) basis functions depending on the inter-particle quantum modes.[17,19] The total wavefunction is then obtained by minimizing the energy functional through the variational principle. Following these ideas, Mátyus and Reiher have very recently developed a new numerical approach,[20] obtaining rotational-vibrational-electronic energy levels with spectroscopic accuracy.

Another branch of non-BO methodologies employs the same strategies and basis-type functions as in standard electronic structure calculations, for the lightest nuclei, fixing the positions of heavier nuclei which are then treated via the BO approximation. An overview of these methodologies has been provided by Sherrill and collaborators[21] and, very recently, by Goli and Shahbazian.[22] They are known by different acronyms, such as multi-component molecular orbital (MCMO), nuclear orbital plus molecular orbital (NOMO), nuclear-electronic orbital (NEO), and *any-particle* molecular orbital (APMO), as described below. A scheme considering the most popular approaches and illustrating their evolution over the time is shown in Figure 1. All of them employ GTFs to expand the one-particle orbitals of electrons and quantum nuclei, as in standard molecular orbital calculations, constructing Slater determinants and permanents for fermionic and bosonic quantum particles, respectively. The zeroth-order electronic-nuclear wavefunction is then written as the product of these determinants and permanents. In what follows, adopting the same terms as used by Sherrill and collaborators,[21] these approaches will be referred to as electronic and nuclear molecular orbital (ENMO) approaches.

To our knowledge, the NOMO method, introduced by Nakai and collaborators in the late 1990s,[23] represents the earliest ENMO-type contribution (see, for example, Ref. 24 for a revision). There, self-consistent mean-field equations

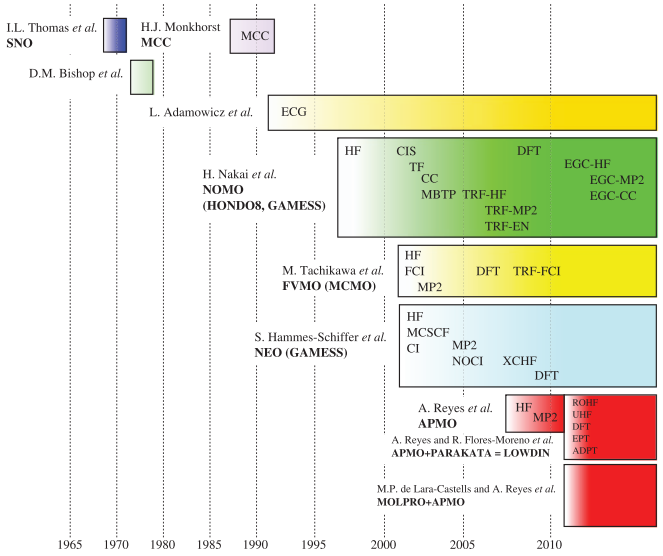

FIG. 1. Scheme illustrating the evolution over the time of methodological and computational ENMO implementations.

for electrons and nuclei were derived in the usual QC notation, and applied using variationally optimized GTFs. Already at the earliest stages of its development, however, the NOMO approach was extended to treat electronic and excited vibrational states with the single configuration interaction (CIS) method,[25] and re-formulated to rigorously remove the center-of-mass motion[26] from the total Hamiltonian (i.e., the translation-free (TF) NOMO version). Moreover, correlation effects were also incorporated by adopting many-body perturbation theory (MBPT) and the CC approach,[27] clarifying the major role of the electron-nucleus correlation. Further developments[24,28–30] allowed to approximately substrate the rotational contribution[29,31] also (i.e., the translation- and rotation-free (TRF) NOMO version[28]). The TRF-NOMO implementation was also extended to incorporate many-body correlation effects with second-order Möller-Plesset (MP2) and Epstein-Nesbet (EN) perturbation theory.[30] More recently, Nakai's group has conducted important progresses towards an accurate description of the electron-nucleus correlation through the incorporation of ECG-type functions (i.e., the ECG-NOMO approach[32–34]). The basic difference between NOMO/HF and ECG-NOMO/HF implementations consists in replacing electronic GTFs with the origin on the nuclear orbital centers by explicit correlated GTF between the electronic and nuclear coordinates.[32] This way, short-range electron-nucleus correlation effects are effectively accounted for. Since the ECG-NOMO/HF method involves the self-consistent resolution of HF-type equations for electrons and nuclei, the conceptual simplicity of the original NOMO/HF implementation is preserved. The latest ECG-NOMO implementation[34] incorporates electronic correlation effects with the MP2 and CC approaches, revealing that the ECG-NOMO method outperforms its TRF-NOMO counterpart.[34]

Another major ENMO-type contribution is the so-called MCMO method (for recent revisions see Refs. 35 and 36). Actually, the origin of this method dates back to the (above mentioned) work by Nakai and collaborators.[23]

Later, Tachikawa and Osamura applied it (then termed the dynamical extended MO method) to hydrogen and lithium hydride molecules.[37] One common characteristic of these contributions is the application of the *fully variational* (FV) treatment to optimize both exponents and center positions of the GTFs (and thus termed the FVMO approach[23,38,39]). Next, Tachikawa was independently involved in further applications[40] and developments[41] of the MCMO method (see Figure 1). This way, the MCMO method approach was extended to incorporate many-body correlation effects with the FCI[41] and MP2 approaches.[42] The highest accurate MCMO method, however, was developed by adopting the TRF formalism from Nakai *et al.*[28] (see above) with the many-body correlation described at FCI level.[43] Hereafter, this approach will be referred to as the FCI *fully variational* MO method.

Parallel computational and methodological developments have been carried out by Hammes-Schiffer's group over the last ten years,[44] with their ENMO-type method termed the NEO approach, which is implemented in the GAMESS suite of programs.[45] Starting with the HF approximation for both electrons and nuclei,[44,46,47] their current implementation allows to include the electron-nuclear correlation either with explicitly correlated Gaussians (the NEO-XCHF and NEO-XCHF2 versions[48,49]) or using variational and perturbative post-HF methods such as non-orthogonal CI (NOCI),[50] multi-configurational self-consistent field (MCSCF), and MP2 approaches.[51] Aimed to describe large molecular aggregates, multi-component density functional theory (DFT), first proposed by Parr *et al.*[52] in the earlier 1980s and later by Shigeta *et al.*[53] and Kreibich and Gross,[54] has been recently included in NOMO,[55,56] NEO,[57] and MCMO[58] implementations. In particular, the Colle-Salvetti functional,[59] originally designed to account for the short-range correlation between the electrons, was extended by Nakai's group[55,56] to describe electron-nucleus correlation effects.

More recently, the any particle molecular orbital APMO code[60–64] was developed. Restricted HF (RHF) equations were implemented in the original code[60] which was further extended to include inter-particle correlations at MP2 level,[61] and to remove the translational contamination at HF level.[65] The main novelty of the APMO implementation lies in its capability of describing systems containing any combination of quantum species (e.g., different isotopes), allowing to deal with exotic species such as positronic and muonic molecules and atoms.[65] Further extensions with the PARAKATA code[66] (the LOWDIN package[67]) allow to describe the quantum particles with the unrestricted-HF approximation and using either DFT or auxiliary perturbation theory (ADPT), and to carry out calculations with electron propagator theory (EPT).[68]

In this paper, we present the first applications of the APMO-MOLPRO interface. Our main goal is to include NQE into standard highly correlated electronic structure calculations using the general-purpose MOLPRO package of programs.[69] The MOLPRO code has a rich tool-box of methodologies to accurately describe both multi-reference or open-shell cases and systems where dynamic correlation effects play an important role. The APMO-MOLPRO implementation enables to perform regular calculations with MOLPRO considering the lightest nuclei as quantum particles, described at RHF level of theory through the APMO code. This implementation is applied to three types of systems: the $^4He_2$ dimer, $[He–H–He]^+$, $[He–D–He]^+$, and $[He–T–He]^+$ isotopomers, and molecular hydrogen along with its isotopomers.

The $^4He_2$ dimer has been chosen as a prototype dispersion-dominated weakly bound system with a van der Waals interaction. We wish to stress that our aim is not to question the validity of the BO approximation in these systems neither the spectroscopic accuracy reached in BO-based studies but to explore whether the incorporation of nuclear quantum effects directly in the electronic structure calculations may speed up the convergence with respect to the level of theory. This issue is worth considering because the accurate description of weakly bound systems at *ab initio* level with post-HF methods (e.g., the coupled-cluster approach) faces the problem of the slow convergence with both the one-electron basis set size and the level of the many-body electron correlation treatment. When applied to dimers of noble gases (see, e.g., Ref. 70 for an extensive analysis), explicitly correlated coupled-cluster methods certainly accelerates the convergence but the improvement is more moderate than that found in other systems. On the other hand, not only the calculation of the potential energy surfaces is challenging but also that of the molecular energy levels and, then, the spectra. We can number the following reasons: (1) the Fermi-Dirac (Bose-Einstein) statistics of the lightest nuclei; (2) their wide (highly anharmonic) amplitude motions; and (3) both the weakly attractive (long-range) and the strongly repulsive (short-range) interaction. The FCI-NO approach was designed to deal with these three problems, showing that the hard-core wall present in the potential energy curves amplifies the short-range nuclear dynamic correlation effects and, therefore, very large nuclear basis sets are necessary to get accurate rotational-vibrational energy levels. Hence, the central question is whether numerical implementations that describes the lightest nuclei and electrons simultaneously could be more efficient, with respect to the level of approximation, in computational spectroscopy of weakly bound systems. Although it is not possible to answer this question in general terms, it is worthwhile to carry out numerical tests, as we will show below.

A second application considers $[He–H–He]^+$ and its isotopomers as weakly bound hydrogen-bonded model systems where the strength of the interaction is intermediate between that of van der Waals and hydrogen bonding. First, we investigate the nuclear basis set convergence of total energies. We have found an important correlation between isotope mass and nuclear density localization. Third, a connection between ENMO- and BO-based pictures is shown by correlating the different density profiles of H, D, and T nuclei with the isotope-mass influence into zero point energies. Finally, the ENMO implementation is applied to molecular hydrogen and its isotopomers with the main objective of comparing with previous results on the same system.

The paper is structured as follows. Section II outlines the methodological approach with the emphasis on the strategy adopted to design the computational APMO-MOLPRO

implementation. Section III presents its application to the above mentioned systems. Section IV closes with a summary and points out possible directions for future applications and extensions.

II. METHODOLOGICAL BACKGROUND

To unify the notations, we first outline the expressions used in a conventional electronic structure calculation at HF level of theory. Considering the particular case of a closed-shell molecule with $\mathcal{N}$ nuclei and N electrons (denoted as e), the RHF wave-function is expressed using Fock space (occupation-number) representation as

$$|\Phi^e\rangle = |n_1 \cdots n_i \cdots n_M\rangle, \tag{1}$$

where M is the total number of spin-orbitals and the occupation number n_i is 1 for N spin orbitals and zero otherwise. The (double occupied) spatial molecular orbitals are constrained to be orthonormal to each other, and can be written as a linear combination of N_{bf} (non-orthonormal) GTFs,

$$\psi_i(\mathbf{r}^e) = \sum_{\mu=1}^{N_{\text{bf}}} C_{\mu i}\chi_\mu(\mathbf{r}^e) \tag{2}$$

with $\mathbf{r}^e$ collectively designating the spatial coordinates of the electrons. The GTFs can be expressed as

$$\begin{aligned}\chi_\mu(\mathbf{r}^e) \propto (x^e - X^\mu)^{l_\mu}(y^e - Y^\mu)^{m_\mu}(z^e - Z^\mu)^{n_\mu} \\ \times \{\exp(-\alpha_\mu(r^e - R^\mu)^2)\},\end{aligned} \tag{3}$$

where $\mathbf{R}^\mu = \{X^\mu, Y^\mu, Z^\mu\}$ specify the coordinates at which the GTFs are centered (the fixed nuclear positions in conventional electronic structure calculations). Since only Cartesian GTFs are implemented within the APMO code, we used also Cartesian GTFs in the MOLPRO electronic structure calculations.

The HF equations can be written in matrix form as

$$\mathbf{FC} = \mathbf{SC}\epsilon \quad \therefore \quad \mathbf{F} = \mathbf{K} + \mathbf{I} + \frac{1}{2}\mathbf{G}, \tag{4}$$

where $\mathbf{K}$, $\mathbf{I}$, and $\mathbf{G}$ are the matrix representations of the electronic kinetic energy, the electron-nuclear attraction, and the electron-electron repulsion, respectively. Explicitly,

$$\begin{aligned}K_{\mu\nu} &= \int \chi_\mu^*(\mathbf{r}^e)\left[-\frac{1}{2}\nabla^2(\mathbf{r}^e)\right]\chi_\nu(\mathbf{r}^e)\,d\mathbf{r}^e, \\ I_{\mu\nu} &= \sum_{\gamma\in\mathcal{N}}\int \chi_\mu^*(\mathbf{r}^e)\left[\frac{Z_\gamma}{|\mathbf{r}^e - \mathbf{r}^\gamma|}\right]\chi_\nu(\mathbf{r}^e)\,d\mathbf{r}^e, \\ G_{\mu\nu} &= \sum_{\lambda,\sigma=1}^{N_{\text{bf}}} P_{\lambda\sigma}\left[(\chi_\mu\chi_\nu\,|\,\chi_\lambda\chi_\sigma) - \frac{1}{2}(\chi_\mu\chi_\sigma\,|\,\chi_\lambda\chi_\nu)\right],\end{aligned} \tag{5}$$

where $\mathbf{P}$ is the first-order reduced density matrix (1-RDM),

$$P_{\mu\nu} = 2\sum_{k=1}^{N/2} c_{\mu k}^* c_{\nu k}. \tag{6}$$

The electronic energy is then written as

$$E_e = tr\left[\mathbf{P}\left(\mathbf{K} + \mathbf{I} + \frac{1}{2}\mathbf{G}\right)\right] + \sum_{I,J\in\mathcal{N}}\frac{Z_I Z_J}{|\mathbf{r}_I - \mathbf{r}_J|}. \tag{7}$$

In a more general case, the molecular system can be divided into the set formed by quantum particles $\mathcal{Q}$ (i.e., the electrons and light nuclei) and the set composed by classical particles $\mathcal{C}$ (e.g., the heavy nuclei). Hereafter, the superscripts α and β will denote different quantum particles. The total wave-function associated with the set $\mathcal{Q}$ can be approximated as a product of the single configuration-state-functions associated with each quantum type,

$$\Psi(\{\mathbf{r}^\alpha\},\{\mathbf{r}^\beta\},\cdots) = \Phi^\alpha(\{\mathbf{r}^\alpha\})\cdot\Phi^\beta(\{\mathbf{r}^\beta\})\cdot\cdot\alpha,\beta\in\mathcal{Q}.$$

For quantum nuclei, we consider a single configuration-state-function where each quantum nucleus is constrained to occupy a different spatial orbital (it corresponds to the highest total spin configuration for nuclei with non-zero spin), using the occupation-number representation,

$$|\Phi^\alpha\rangle = \left|n_1^\alpha \cdots n_i^\alpha \cdots n_{M^\alpha}^\alpha\right\rangle, \tag{8}$$

where M^α is the number of (spin) orbitals defining the Hilbert space of the quantum particle with index α, and n_i^α is either 0 or 1 for quantum nuclei. It should be noticed that this condition is imposed because of the lack of nuclear correlation within the current implementation.

The molecular orbital of any quantum particle ψ^α is expressed as a linear combination of GTFs,

$$\psi_i^\alpha(\mathbf{r}^\alpha) = \sum_{\mu=1}^{N_{\text{bf}}^\alpha} C_{\mu i}^\alpha\chi_\mu^\alpha(\mathbf{r}^\alpha). \tag{9}$$

The matrix expression of the HF equation associated with each quantum particle α reads

$$\begin{aligned}\mathbf{F}^\alpha\mathbf{C}^\alpha &= \mathbf{S}^\alpha\mathbf{C}^\alpha\epsilon^\alpha \\ \mathbf{F}^\alpha &= \mathbf{K}^\alpha + \mathbf{I}^\alpha + \mathcal{J}^\alpha + \frac{1}{\eta^\alpha}\mathbf{G}^\alpha,\end{aligned} \tag{10}$$

where the average interaction between α and the other quantum species (β) is given by the term $\mathcal{J}^\alpha$. Explicitly, the matrix elements may be written as

$$\begin{aligned}K_{\mu\nu}^\alpha &= \int \chi_\mu^{\alpha*}(\mathbf{r}^\alpha)\left[-\frac{1}{2M_\alpha}\nabla^2(\mathbf{r}^\alpha)\right]\chi_\nu^\alpha(\mathbf{r}^\alpha)\,d\mathbf{r}^\alpha, \\ I_{\mu\nu}^\alpha &= \sum_{\gamma\in\mathcal{C}}\int \chi_\mu^{\alpha*}(\mathbf{r}^\alpha)\left[\frac{Z_\alpha Z_\gamma}{|\mathbf{r}^\alpha - \mathbf{r}^\gamma|}\right]\chi_\nu^\alpha(\mathbf{r}^\alpha)\,d\mathbf{r}^\alpha, \\ \mathcal{J}_{\mu\nu}^\alpha &= \sum_{\alpha\neq\beta}\sum_{\lambda,\sigma=1}^{N_{\text{bf}}^\beta} P_{\lambda\sigma}^\beta\left(\chi_\mu^\alpha\chi_\nu^\alpha\middle|\chi_\lambda^\beta\chi_\sigma^\beta\right), \\ G_{\mu\nu}^\alpha &= \sum_{\lambda,\sigma=1}^{N_{\text{bf}}^\alpha} P_{\lambda\sigma}^\alpha\left[\left(\chi_\mu^\alpha\chi_\nu^\alpha\middle|\chi_\lambda^\alpha\chi_\sigma^\alpha\right) \pm \frac{1}{\eta^\alpha}(\chi_\mu^\alpha\chi_\sigma^\alpha|\chi_\lambda^\alpha\chi_\nu^\alpha)\right].\end{aligned} \tag{11}$$

Here, M_α denotes the mass of the quantum particle with index α and the sign $\pm$ corresponds to the bosonic/fermionic nature of this particle. η_α defines the occupation number of a given spatial orbital (i.e., $\eta_\alpha = 1$ for the quantum nuclei considered here) so that the 1-RDM takes the form

$$P^\alpha_{\mu\nu} = \eta^\alpha \sum_{k=1}^{N_{\rm occ}} c^{\alpha *}_{\mu k} c^\alpha_{\nu k}. \tag{12}$$

In the following, we consider molecular systems composed by only one class of quantum nuclei (denoted as n) with charge $+Z_n e$ and mass M_n; then N_n refers to the number of quantum nuclei. A practical calculation starts with the solution of Eq. (4) for the electrons considering both classical and quantum nuclei as fixed point charges within the BO approximation. Next, the electronic 1-RDM, $\mathbf{P}^e$, is employed to calculate the term that couples electronic and nuclear densities $\mathcal{J}^n$, see Eq. (11). Equation (10) is then solved for the quantum nuclei, and the whole process is iterated until convergence. The total energy of the *pseudo*-system composed by quantum particles, that further serves as an effective potential for the classical nuclei, can be written as

$$E = \sum_{\alpha\in\mathcal{Q}} \mathrm{tr}[\mathbf{P}^\alpha \mathbf{F}^\alpha] + \sum_{\gamma,\rho\in\mathcal{C}} \frac{Z_\gamma Z_\rho}{|\mathbf{r}^\gamma - \mathbf{r}^\rho|}, \tag{13}$$

and the electronic energy is conveniently defined as

$$E_e = \mathrm{tr}\left[\mathbf{P}^e\left(\mathbf{K}^e + \mathbf{I}^e + \mathcal{J}^e + \frac{1}{2}\mathbf{G}^e\right)\right] \tag{14a}$$

$$+\mathrm{tr}\left[\mathbf{P}^n\left(\mathbf{I}^n + \frac{1}{\eta^n}\mathbf{G}^n\right)\right] \tag{14b}$$

$$+\frac{1}{2}\left[\mathrm{tr}(\mathbf{P}^n\mathcal{J}^n) - \mathrm{tr}(\mathbf{P}^e\mathcal{J}^e)\right] \tag{14c}$$

$$+\sum_{\gamma,\rho\in\mathcal{C}} \frac{Z_\gamma Z_\rho}{|\mathbf{r}^\gamma - \mathbf{r}^\rho|}, \tag{14d}$$

where the term (14c) is included to avoid the double-counting of the nuclear-electron interaction energy. Also, we notice that the nuclear kinetic energy term ($\mathrm{tr}[\mathbf{P}^n\mathbf{K}^n]$) is separated from the expression of the electronic energy. In the infinite-nuclear-mass limit, the terms $\mathbf{P}^\alpha\mathbf{I}^\alpha$ and $\frac{1}{2}\mathbf{P}^\alpha\mathbf{G}^\alpha$, become the Coulomb repulsion between classical nuclei

$$\begin{aligned}
\mathrm{tr}\left(\mathbf{P}^n\mathbf{I}^n\right) &\xrightarrow[M_n\to\infty]{} \sum_{I=1}^{\mathrm{N}_n}\sum_{\gamma\in\mathcal{C}} \frac{Z_n Z_\gamma}{|\mathbf{r}^n_I - \mathbf{r}_\gamma|}, \\
\frac{1}{\eta^n}\mathrm{tr}\left(\mathbf{P}^n\mathbf{G}^n\right) &\xrightarrow[M_n\to\infty]{} \sum_{I=1}^{\mathrm{N}_n-1}\sum_{J=I}^{\mathrm{N}_n} \frac{Z_n Z_n}{|\mathbf{r}^n_I - \mathbf{r}^n_J|}.
\end{aligned} \tag{15}$$

Similarly, the expression for the electronic energy becomes identical to that in standard electronic structure calculations. It is important to realize that the electronic energy, as defined in Eq. (14), allows to get an effective *potential energy surface* (i.e., the electronic energy as a function of the relative positions between the nuclear GTFs centers). The electronic energy thus represents the expectation value of the full Hamiltonian minus the nuclear kinetic energy, as in standard BO calculations. Typically, an ENMO-type calculation starts with the centers of the nuclear GTFs at the fixed nuclear positions in preliminary BO calculations.

By comparing Eqs. (7) and (14), it is clear that we can make the following mappings:

$$\begin{aligned}
\mathbf{K} &\Leftarrow \mathbf{K}^e, \\
\mathbf{G} &\Leftarrow \mathbf{G}^e, \\
\mathbf{I} &\Leftarrow \mathbf{I}^e + \mathcal{J}^e, \\
\sum_{I,J\in\mathcal{N}} \frac{Z_I Z_J}{r_{IJ}} &\Leftarrow \mathrm{tr}\left[\mathbf{P}^n\left(\mathbf{I}^n + \frac{1}{\eta^n}\mathbf{G}^n\right)\right] \\
&\quad + \frac{1}{2}[\mathrm{tr}(\mathbf{P}^n\mathcal{J}^n) - \mathrm{tr}(\mathbf{P}^e\mathcal{J}^e)] \\
&\quad + \sum_{\gamma,\rho\in\mathcal{C}} \frac{Z_\gamma Z_\rho}{|\mathbf{r}^\gamma - \mathbf{r}^\rho|}.
\end{aligned} \tag{16}$$

From these mappings, it follows that the bare Coulomb interaction between the electrons and the quantum nuclei is replaced by a dressed Coulomb interaction between the electrons and the quantum nuclear charge density, as given by the term $\mathcal{J}^e$. This is schematically illustrated in Figure 2. The nuclei are represented by a distribution $\rho(\mathbf{r}^n - \mathbf{R}^n)$ centered in the clamped nuclear positions from standard BO calculations, $\mathbf{R}^n$. Once again, in the infinite-nuclear-mass limit, the nuclear distribution tends to a delta-type function $\delta(\mathbf{R}^n)$, with the electronic energy (see Eq. (14)) having the same expression as in the BO approximation (see Eq. (7)). From the mappings in Eq. (16), it is clear that the inclusion of electronic correlation into the HF equations for the quantum nuclei can be accomplished by substituting the HF electronic 1-RDM by its correlated counterpart, obtained using the MOLPRO code. Next, this correlated density matrix is introduced into the

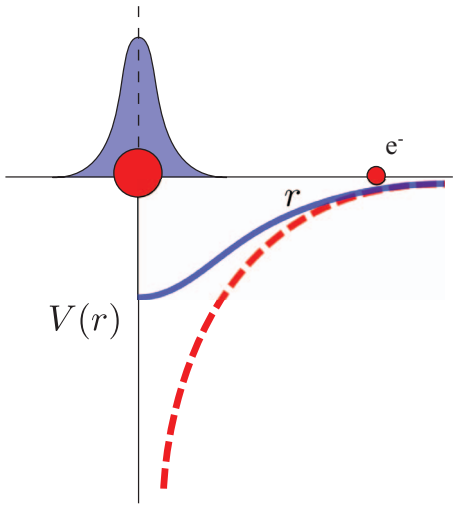

FIG. 2. Schematic illustration of the electrostatic interaction $V(r)$ among a reference electron (highlighted with a small circle) and a nucleus represented as either a fixed point charge within the BO approximation (highlighted with a large circle) or a Gaussian charge distribution with its center located at the position of the fixed nucleus in BO calculations.

coupling term $\mathcal{J}^{\alpha}$ from Eq. (11). The APMO code is then run to solve the Fock equations associated with the quantum nuclei, obtaining a new nuclear charge density. Correlated electronic-structure-like calculations with MOLPRO and HF calculations with APMO are then iterated to achieve self-consistency. The full details of the computational APMO-MOLPRO implementation are available upon request to the authors.

III. APPLICATIONS

We first apply the APMO-MOLPRO implementation to the $^4He_2$ dimer which is a prototype of a weakly bound system. A second application deals with the $[He–H–He]^+$, $[He–D–He]^+$, and $[He–T–He]^+$ isotopomers as a model where the strength of the interaction is intermediate between that of van der Waals and hydrogen bonding systems. Finally, the molecular hydrogen and its isotopomers are considered.

A. A model of weakly interacting system: The $^4He_2$ dimer

Our calculations were performed using the singly augmented version of the correlation-consistent polarized aug-cc-pVQZ basis set (referred to as AVQZ) developed by Dunning and collaborators[71,72] for the electrons and a $2s2p$ basis set for the nuclei. The CC singles and doubles, and noniterative triples [CCSD(T)] method was applied with an integral threshold of 10^{-14} a.u. We followed the counterpoise (CP) procedure proposed by Boys and Bernardi[73] to account for the intramolecular basis set superposition error (BSSE) for both electrons and nuclei. For comparison, additional standard electronic structure CCSD(T) calculations with the double diffusely augmented d-aug-cc-pV6Z basis set (DAV6Z) were also performed. The nuclear basis set was calibrated through the gradual addition and optimization of exponent of s and p GTFs following the sequence $1s \rightarrow 2s \rightarrow 2s\ 1p \rightarrow 2s\ 2p$. Each exponent optimization step involved a simultaneous geometry optimization. The simplex algorithm was used for the exponents optimization with an accuracy threshold of 10^{-6} a.u. As a final step, a global re-optimization of all the exponents α and the geometry was performed. This procedure resulted in the following values for the optimized exponents: 171.9559 ($1s$), 216.0468 ($2s$), 238.0624 ($1p$), and 250.0442 ($2p$).

Fixing the He–He internuclear distance, we started with a standard CCSD(T) calculation with MOLPRO (i.e., clamping the He nuclei). Next, the electronic CCSD 1-RDM was used to calculate the nuclear-electronic coupling matrix $\mathcal{J}^{n}$ (see Eq. (11)) and the Fock equation associated with the nuclei and including the mean-field generated by the electronic charge density, was solved with the APMO code, with the centers of the nuclear GTFs kept fixed at the positions of the clamped nuclei in the preliminary BO calculations. This was followed by a CCSD(T) calculation for the electrons with MOLPRO including the NQE through the nuclear HF 1-RDM. CCSD(T) and HF calculations for the electrons and the nuclei were then run iteratively until self-consistency. This procedure is repeated for different distances between the nuclear GTFs centers. Figure 3 shows the resulting effective potential energy curve (PEC) (highlighted in red). For the sake of clarity, Table I summarizes the main results (well-depths and minimum energy positions).

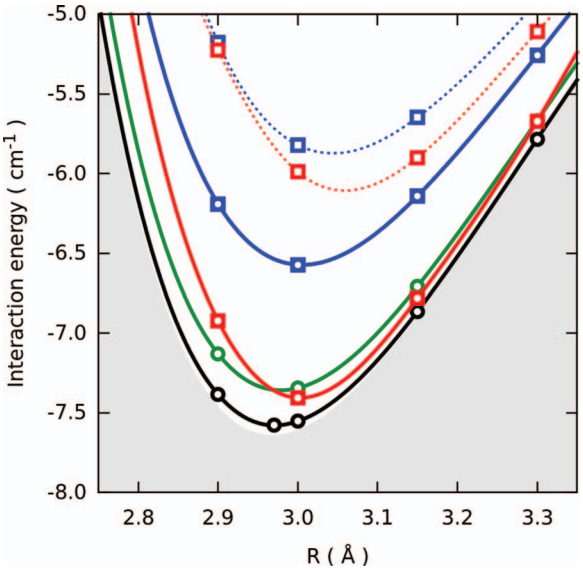

FIG. 3. $^4He_2$ dimer potential energy curves. APMO-MOLPRO CCSD(T){CCSD}/AVQZ:2s2p (red solid line); MOLPRO CCSD(T)/AVQZ (blue solid line); MOLPRO CCSD(T)/DAV6Z (green); MOLPRO FCI/DAV6Z (black) from Ref. 77. The reference potential energy curve from Ref. 74 is shown as a shaded area. The CCSD entry in APMO-MOLPRO CCSD(T){CCSD}/AVQZ indicates that only the CCSD correlated 1-RDM has been employed into the HF equations for the nuclei. APMO-MOLPRO CCSD(T){CCSD}/AVTZ:2s2p (red dashed line) and MOLPRO CCSD(T)/AVTZ (blue dashed line) results are also shown.

Naturally, a rigorous non-BO calculation would provide directly the energy D_0 and wave-function of the $^4He_2$ weakly bound state that have been experimentally observed (i.e., without relying on a PEC). Due to the highly delocalized nature of this state ($\langle R \rangle$ 47.1 ± 0.5 Å from Ref. 74), however, a much larger nuclear basis set would be necessary to carry out such calculations, along with the separation of the center-of-mass operator from the molecular Hamiltonian and the inclusion of the electron-nuclear correlation. Extremely accurate estimations of D_0 or $\langle R \rangle$ values have been very recently provided by Cencek *et al.* (see Ref. 74) by calculating the nuclear wave-function supported by the helium dimer potential. This PEC was obtained through very accurate BO calculations including post-BO adiabatic and relativistic corrections as well as quantum electrodynamic effects. Here, by computing an effective helium dimer potential, we adopt an approach

TABLE I. Well-depths (E^{int}_{min}) and minimum energy positions (R_{min}) of the $^4He_2$ dimer potential energy curves shown in Fig. 3.

	R_{min}(Å)	E^{int}_{min}(cm^{-1})
AVTZ: BO/ENMO	3.04/3.06	− 5.8729/−6.1065
AVQZ: BO/ENMO	3.00/3.00	− 6.5727/−7.4054
DAV6Z(BO):[a] CCSD(T)/FCI	2.98/2.97	− 7.3580/−7.5785
Reference 74	2.97	− 7.6429

[a]Reference 77.

which is somewhat different from other applications within the ENMO framework. As already mentioned, our goal is to estimate if the inclusion of quantum nuclear effects would affect the level of theory required to correctly account for dynamic correlation in electronic structure calculations, and, more particularly, the flexibility of the orbital space for an adequate description of the dispersive interaction. Our interpretation follows the lines of BO method using floating Gaussian orbitals,[75,76] with the electrostatic attractive field generated by vibrating nuclei as the guiding function for the electronic orbitals, see also below.

In Figure 3, the APMO-MOLPRO CCSD(T) PEC (solid red line) is compared with standard CCSD(T) electronic structure calculations using the same (AVQZ) electronic basis set (solid blue line) or the much larger DAV6Z basis set (highlighted in green). The most accurate PEC from Ref. 74 is also shown as a shaded area. For comparison purposes, the FCI potential obtained using the DAV6Z basis set from Ref. 77 is also displayed (black line). This FCI potential provides a bound state for the ^{4}He dimer that disappears when its depth-well is reduced by a mere 0.02% (e.g., the FCI PEC with the AVQZ basis fails to provide a bound helium dimer state). Although this FCI potential is very close to the reference potential from Ref. 74, the associated D_0 value is about 0.5 mK above the best estimation at present ($D_0 = 1.62 \pm 0.03$ mK from Ref. 74).

Let us now compare our ENMO results to those obtained from standard electronic structure calculations. From Figure 3, it can be noticed that the APMO-MOLPRO CCSD(T) potential with the AVQZ basis set is very close to that obtained through standard CCSD(T) calculations using the much larger DAV6Z basis set (110 vs. 476 Cartesian GTFs). In contrast, the well-depth of the potential from conventional CCSD(T) calculation with the AVQZ basis set is 0.83 cm^{-1} higher (see Table I). This result demonstrates that the inclusion of NQE allows to effectively reduce the electronic basis set size. This can be understood by considering that the Kato's (electron-nuclear) cusp condition[78] becomes somehow smoothed out when a fixed point charge is replaced by a finite nuclear charge distribution (see Figure 2), taking away the divergence of the electron-nucleus Coulomb potential as $-Z/r$ when r goes to zero. On the other hand, when using Gaussian-type orbitals whose gradient is zero at the origin, the Kato's cusp condition is not satisfied.[79] Moreover, it seems clear that the nuclear charge distribution shown in Figure 2 is capable to push electronic density out into regions associated with the dispersive interaction, thus relaxing the strong requirements for the GTFs (intrinsically unable to properly describe the electron-electron cusp also) basis set size. In other words, as the He nuclei approach each other, their associated electronic clouds become more diffuse and interactive, increasing the dispersive effect. On the contrary, a fixed point charge attracts more electronic density to its position. The electronic orbitals become thus effectively more flexible in the scenario of a vibrating nucleus. These arguments are similar to those presented in Ref. 76 to explain the reasons why Diffusion Monte Carlo (DMC) calculations with floating spherical GTFs in the guiding function provide better results than their standard GTFs-type counterparts. On the other hand, ENMO calculations with the quantum nuclei described through relatively narrow amplitude GTFs could be phenomenologically identified with standard BO calculations using floating electronic orbitals.[76] Thus, the most important insight that can be extracted from the consideration of finite-mass effects in a model system for the dispersion interaction is that the requirements for the electronic structure calculations are less stringent than in the infinite-nuclear-mass limit.

TABLE II. Interaction energy differences $\Delta\mathcal{E}$ (in cm^{-1}) between APMO-MOLPRO CCSD(T){CCSD}/AVQZ:2s2p and MOLPRO CCSD(T)/AVQZ calculations (second column) as a function of the distance between GTFs nuclear centers R_{He-He}, in Å (first column). Third column: Diagonal adiabatic correction $V_{ad,int}^{corr}$ (in cm^{-1}) for $^4He_2$ as a function of the He–He inter-nuclear distance R_{He-He}, in Å.

R_{He-He} (Å)	$\Delta\mathcal{E}$ (cm^{-1})	$V_{ad,int}^{corr}$ (cm^{-1})[a]
1.85	56.2514	0.2962
2.15	15.4504	0.0614
2.40	4.0442	0.0086
3.00	− 0.8331	− 0.0061
3.80	− 0.0441	− 0.0020

[a]Reference 74.

We notice that the interaction energy difference between BO- and ENMO-type calculations (see Table II) should not be confused with the diagonal adiabatic correction to the BO energies. This is apparent from the definition of the latter as the expectation value of the nuclear kinetic energy operator,[80]

$$V_{ad}^{corr} = \left\langle \Phi_{BO}^{e} \middle| -\sum_{I} \frac{\nabla_I^2}{2M_I} \Phi_{BO}^{e} \right\rangle, \tag{17}$$

and taking into account that the kinetic nuclear energy is subtracted to obtain the interaction energy within the ENMO framework. By construction, the term V_{ad}^{corr} is a finite-mass adiabatic correction to the electronic energy only, while the ENMO approach includes the influence of these finite-mass effects onto the electronic wave-function itself. As reported by Cenket *et al.*,[74] the inter-nuclear dependence of the finite-mass correction $V_{ad,int}^{corr}$ can be calculated by subtracting the corresponding (mass-polarization) term from two isolated helium atoms. Interaction energy differences between BO- and ENMO-type calculations are compared with reference $V_{ad,int}^{corr}$ values from Ref. 74 for a selected set of inter-nuclear distances. As can be seen from Table II, the energy difference obtained by the inclusion of finite-mass effects with the ENMO approach is more than two orders of magnitude larger than the adiabatic correction around the minimum of the potential energy curve. Both energy differences are positive at very short inter-nuclear distance, change their sign close to the minimum, and approach zero at large distances. Thus, the inclusion of finite-mass effects tends to stabilize the ^{4}He dimer, as expected.

So far, our goal has been the analysis of NQE for highly correlated electronic energies. Let us now focus on the nuclear response to these electronic correlation effects. For this purpose, Table III lists the nuclear relaxation energies $\Delta\mathcal{E}_{rex}^{nuc}$ obtained by replacing the HF electronic 1-RDM by its correlated counterpart, calculated with the CCSD approach. As apparent

TABLE III. Nuclear relaxation energies $\Delta\mathcal{E}_{rex}^{nuc}$ (in cm^{-1}) as a function of the distance between GTFs nuclear centers, R_{He-He}, in Å (first column). Second (third) column: APMO-MOLPRO CCSD(T){CCSD}/AVTZ:2s2p (CCSD(T){CCSD}/AVQZ:2s2p) results.

	$\Delta\mathcal{E}_{rex}^{nuc}$ (cm^{-1})	
R_{He-He} (Å)	AVTZ	AVQZ
2.30	−1.1522	−1.1105
2.70	−0.7638	−0.7001
3.40	−0.1141	−0.0768
3.80	−0.0680	−0.0088

from this table, the nuclear response to the electronic correlation becomes increasingly more pronounced as the distance between GTFs nuclear centers decreases. Then, at distances shorter than 2.4 Å, the nuclear relaxation energy reaches values larger than -1.0 cm^{-1}, lowers to about -0.5 cm^{-1} close to the minimum, and approaches zero at 3.8 Å. From Table III, it can be also seen that the electronic AVQZ and AVTZ basis sets provide very similar values with nuclear relaxation energy differences below 0.07 cm^{-1}. Contrarily, electronic interaction energies obtained using BO- and ENMO-type calculations with the AVTZ basis set are fairly inaccurate (see Fig. 3 and Table I). The inclusion of NQE certainly improves the well-depth value calculated with the AVTZ basis as compared to the reference one[74] and the same general trends upon augmentation of the basis set size are found in both BO- and ENMO-type calculations. The current APMO-MOLPRO interface is implemented for up to *g*-type Gaussian functions, that corresponds to the VQZ-type basis for main group elements. Work is in progress to implement *h*- and *i*-type functions that will allow to use up to V6Z basis sets. Upon increasing the nuclear basis sets size, including electron-nuclear correlation, and separating the center-of-mass motion, a second regime would be eventually reached in which the inter-nuclear quantum mode itself is correctly described. Concerning the inclusion of short-range nuclear correlation effects, it has been shown through BO-based studies[6] with the FCI-NO approach that their proper description in doped ^{3}He clusters is crucial in getting physically meaningful results, as the pairing found for ^{3}He and the quasi-degeneracy of different nuclear spin-states. In turn, this quasi-degeneration renders the spectra of probe molecules inside ^{3}He very congested[3,81] at temperature for which spinless ^{4}He droplets are superfluid and the guest molecule spectrum displays sharp rotational lines. As already mentioned, very large one-particle basis sets and special diagonalization techniques are necessary to describe these short-range correlation effects with FCI-NO (BO-based) calculations[6] due to the sharply repulsive He–He potential at short distances that raises much more steeply compared to the Coulomb potential. As follows from present results, however, the requirements for the one-particle basis set and the many-particle correlation treatment are less demanding when nuclei and electrons are treated simultaneously. In any case, the inclusion of the nuclear correlation is necessary to relax the maximum spin condition for the nuclear (^{3}He) wave-function.

Summarizing, it is necessary to develop nuclear basis sets better tailored to describe the inter-nuclear motion in conjunction with the separation of the center-of-mass motion, and practical approaches to include the electron-nuclear correlation. For a diatomics like $^4He_2$, if the position of one nucleus is frozen (infinite-nuclear-mass limit), the mass of the second nucleus is fixed to the reduced mass, and the center of the second nucleus GTFs is also optimized, it would be possible to obtain an estimation of the zero point energy D_0, since the separation of the center-of-mass motion is already accounted for. In our case, this procedure leads to the lowering of the nuclear kinetic energy by about 0.03 a.u. Still, it is important to realize that one-centered GTFs are unable to account for the highly delocalized nature of the $^4He_2$ wave-function. For this purpose, it would be suitable to use multi-centered Gaussian functions adding nuclear *ghost* GTFs. This strategy is somehow reminiscent to the addition of midbond GTFs in the electronic basis sets to saturate the dispersion interaction. It also resembles the "distributed Gaussian functions" (DGF) method of Hamilton and Light[82] for solving multi-dimensional vibrational problems, as applied[83] to $^4He_2$ and $^4He_3$. Since the APMO implementation already enables the use of nuclear *ghost* GTFs, the problem would translate in designing efficient algorithms to distribute the GTFs centers. We notice that the DGF method was proposed to deal also with excited vibrational states.[82] Concerning the inclusion of the inter-particle correlation, the transcorrelated Hamiltonian approach[84] seems to be quite attractive. By using a single determinant (permanent) Jastrow *ansatz*, HF-like equations are obtained and, therefore, this approach seems to be well-suited to interfaces with standard electronic structure codes.

B. $[He–H–He]^+$ and its isotopomers

As a second application, we studied the $[He–H–He]^+$, $[He–D–He]^+$, and $[He–T–He]^+$ isotopomers. These are model systems in which the interaction strength is remarkably influenced by the nuclear delocalization of the central nucleus (i.e., H, D, or T). As in previous works within either the BO[85,86] or the ENMO frameworks,[49,61] a symmetric linear structure for the $[He–H–He]^+$ system was considered. The two lateral He nuclei were treated classically and the central nucleus was considered as a quantum particle. Specifically, the quantum nucleus was described with a 5*spd* basis set of GTFs, while the CCSD(T) method and the AVQZ basis set were employed for the electrons. The nuclear GTFs were located at the midpoint between the two He nuclei. Taking into account the small difference between the masses of hydrogen and helium nuclei, a rigorous non-BO calculation should treat both nuclei equivalently. However, we have chosen this approach as it allows for a direct comparison with results obtained earlier using similar methods.[49,61]

The exponents of the nuclear GTFs were obtained using an even-tempered set.[69] The same set of basis functions was employed for all isotopes. Following the strategy proposed by Nakai,[26] the exponents of nuclear GTFs with non-zero orbital angular momentum quantum numbers were set to the same values as for the *s*-type GTFs. Figure 4 shows the convergence

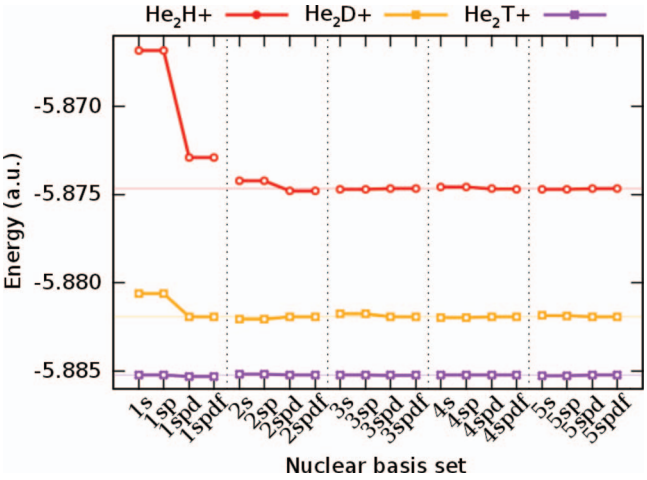

FIG. 4. Convergence of the total energy upon addition of nuclear GTFs for the $[He–H–He]^+$ system and its isotopomers.

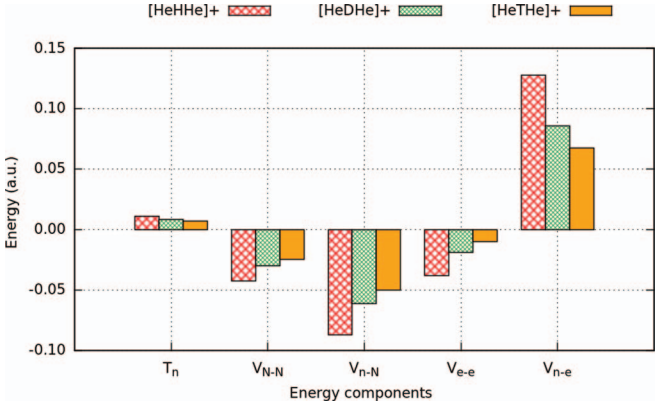

FIG. 5. Decomposition analysis of the energy terms associated with the $[He–H–He]^+$, $[He–D–He]^+$, and $[He–T–He]^+$ systems (see text).

of the total energies as a function of the number of primitive GTFs. These energies were obtained by fixing the He–He internuclear distance at the optimized value in standard CCSD(T) calculations. As a first step, the exponent of a single 1*s* GTF was optimized variationally for each isotope. The average exponents of the 1*spdf* GTFs in the even-tempered sets were set to these optimized values. When only one *s*-type function is employed, the three systems share the same nuclear density distributions. Therefore, the pronounced isotope mass dependence of the total energy (see Figure 4) comes directly from the $1/M_n$ term in the kinetic energy matrix (see Eq. (11)). The further addition of nuclear GTFs enables a differential localization of the nuclear densities depending on the isotope mass, reducing thus the total energy differences, see Figure 4. It is clearly apparent that a 5*spd* basis set suffices to get convergent total energy values for the three complexes.

As a second step, the geometry of the system was optimized using the 5*spd* basis set. The resulting total energy values were −5.8754, −5.8823, and −5.8855 a.u. for the $[He–H–He]^+$, $[He–D–He]^+$, and $[He–T–He]^+$ complexes, respectively. As expected from the higher level of theory adopted here, these energies are lower (∼0.04 a.u.) than those obtained with the APMO-MP2 method.[61] To gain further insight into isotope-dependent effects, we calculated the average values of the quantum nucleus kinetic energy T_n, the electronic repulsion V_{e-e}, the He–He repulsion V_{N-N}, the repulsion energy between the central nucleus and the classical He nuclei V_{n-N}, and the electron-central nucleus attraction V_{n-e}. The differences between the values obtained within the ENMO framework for the three systems and those resulting from standard CCSD(T) calculations for the $[He–H–He]^+$ complex are shown in Figure 5. Table IV lists the average internuclear distance $\langle R_{X-He}\rangle$ with the optimized molecular geometry, while the nuclear density distributions are displayed in Figure 6.

We observed isotope mass effects similar to those found in Ref. 61. They can be understood by considering: (1) the isotope mass increase from protium to tritium; (2) the concomitant localization of the nuclear densities (see Figure 6); and (3) the resulting compression of the electronic densities. Naturally, the nuclear kinetic energy increases if the isotope mass decreases, $1/M_n$ increases. Once again, as apparent from Figure 2, the most attractive electron-nuclear interaction corresponds to the infinite nuclear mass limit. Therefore, for heavier central nucleus, the average value of V_{n-e} is larger. On a contrary, the Coulomb repulsion between the central nucleus and the He nuclei is larger as the former becomes more localized (see the energy differences associated with the V_{n-N} component in Figure 5). Also, it can be noticed that the average V_{e-e} interaction becomes less repulsive as the central nucleus becomes more delocalized. As discussed above for the ^{4}He dimer, the electronic density is more sparse when a fixed point charge is replaced by a nuclear charge density, making their average interaction less repulsive. Considering the results presented in Table IV, we mention that the equilibrium He–H bond distance obtained with conventional electronic structure calculations (0.9249 Å from Table IV) agrees very well with previous calculations using highly correlated methods (i.e., 0.925 Å from Ref. 86), indicating that the electronic correlation is properly described. We can also notice from Table IV the shortening of the average internuclear distances $\langle R_{X-He}\rangle$ as the central nucleus becomes more localized, making the He–He interaction more repulsive (see Figure 5). On the other hand, the values of the Mulliken charges (see Table IV) are smaller than those obtained through a standard BO-based calculation, reflecting the delocalization of the electronic densities after the inclusion of finite-mass

TABLE IV. Average internuclear distances $\langle R_{X-He}\rangle$ (in Å), differences between $\langle R_{X-He}\rangle$ values obtained at HF and CCSD(T) levels of theory ($\Delta\langle R_{X-He}\rangle$, in Å), and Mulliken charges on the central nucleus (in a.u.) obtained for the $[He–X–He]^+$ isotopomers (i.e., X = H, D, and T) in the present work.

	$\langle R_{X-He}\rangle$ (Å)	$\Delta\langle R_{X-He}\rangle$ (Å)	Mulliken
	0.9608		0.387
$He–H–He^+$	0.9249[a]	0.0144[a]	0.635[a]
	0.9631[b]		
$He–D–He^+$	0.9498	0.0094	0.399
$He–T–He^+$	0.9451	0.0075	0.409

[a] Values obtained with conventional electronic structure calculations.
[b] APMO-MP2 value from Ref. 61.

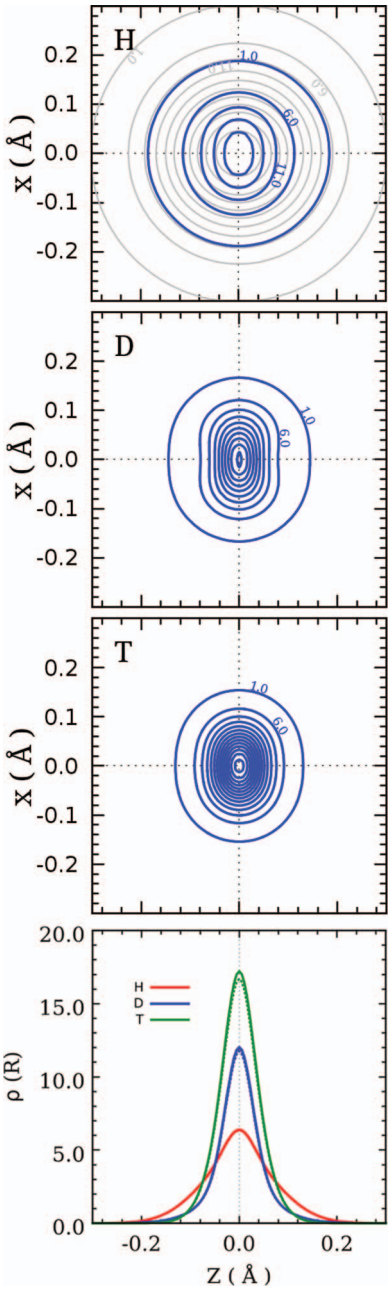

FIG. 6. Three top panels: Contour plots of the nuclear density distributions of $[He–X–He]^+$ for X = H, D, and T, on a plane containing the He–He internuclear axis (the z axis). The distances are given in Å. Adjacent contours are separated by 5.0 $Å.^{-2}$ A model spherical density distribution (grey color) has been superimposed to the protonic density in the $[He–H–He]^+$ system. Bottom panel: One-particle protonic density distributions, with the electrons described at either CCSD(T) (solid lines) or HF (dotted lines) levels of theory, calculated along the He–He internuclear axis of $[He–X–He]^+$ (with the origin located in the middle of the two He nuclei) for X = H, D, and T.

effects, as already discussed for the helium dimer. These effects become more pronounced as the nuclear mass decreases. Within standard BO-based theory, this is explained by considering the PES anharmonicity and the wider amplitude zero-point motions attained by the lightest isotopes (see, for example, Ref. 87). Within the ENMO approach, the latter trend is reflected in more delocalized nuclear densities as the nuclear mass decreases (see Figure 6). Interestingly, the protonic densities are rather isotropic in contrast to those attained by deuteron and triton nuclei, which are more confined in the direction of the internuclear He–He axis. In the standard BO-based picture, the heaviest tritium nuclear density shows the most anisotropic shape that adapts better to the anharmonic potential due to its smaller zero point energy. Physical insights into the system are thus gained directly with ENMO-type calculations before resorting to the quantum treatment of the nuclear motion on the electronic potential energy surface. The isotropic character of the protonic densities could be correlated with a quasi-degeneracy of zero point energies for asymmetric stretching and bending normal modes of the electronic ground state in standard BO-based calculations. Very similar energies for stretching and bending frequencies were found by Ko *et al.* in Ref. 49 using a single 1s GTF. The inclusion of GTFs with higher angular momentum quantum numbers in the present work enables a more balance description of stretching and bending modes. Also, previous works have shown that the vibro-rotational energy levels supported by the $[He–H–He]^+$ PES do not correspond to any particular mode but to a combination of them.[87] Focusing on the comparison with previous works using ENMO approaches, it can be noticed that our value for $\langle R_{X-He} \rangle$ is quite close to that obtained in Ref. 61 using the APMO-MP2 method (see Table IV). More significant differences are found, however, by comparing the protonic density distribution from the present work (see the bottom panel of Fig. 6) and that obtained using the NEO-XCHF2 method (see Fig. 1 from Ref. 49). Thus, the inclusion of the electron-nuclear correlation with the NEO-XCHF2 approach leads to a higher degree of delocalization for the protonic densities, as discussed in previous works for the same system.[49,61] On the contrary, as shown in the bottom panel of Fig. 6, nuclear density distributions at the equilibrium geometry obtained with the electrons described at HF and CCSD levels are almost indistinguishable. The equilibrium geometry itself, however, is affected by the nuclear response to the electronic correlation. This is clearly reflected in the isotope dependence of the differences between the $\langle R_{He\text{-}X} \rangle$ expectation values obtained at HF and CCSD(T) levels of theory, as shown in Table IV ($\Delta\langle R_{He\text{-}X} \rangle$ values). Thus, for protium, the enlargement of the average He–H distance at CCSD(T) level is about twice as larger than for tritium. The nuclear response to the electronic correlation is thus more pronounced for the lightest isotope, as expected.

C. Isotopomers of molecular hydrogen: Prototype model systems

The isotopomers of molecular hydrogen are prototype model systems to test the robustness of ENMO approaches and computational implementations[43,60] by virtue of their relative simplicity. The highly accurate non-BO calculations on these systems have been carried out by Adamowicz and collaborators[88–91] using an internal rotationally invariant molecular Hamiltonian and explicitly correlated GTFs, and including relativistic corrections to the resulting energies. These works thus provide reference values that can be used to test the accuracy of our results.

We have performed ENMO calculations applying a FCI (HF) treatment for the electrons (nuclei) of H_2, HD, HT,

TABLE V. Average internuclear distances $\langle R_{n-n} \rangle$ (in Å) obtained for molecular hydrogen and its isotopomers.

	HF:HF[a]	HF:FCI[b]	Non-BO	Experimental[c]
H_2	0.7765	0.7628	0.7666[d]	0.7511
HD	0.7698	0.7602	0.7632[e]	0.7498
HT	0.7668	0.7599		0.7493
D_2	0.7632	0.7598	0.7591[f]	0.7484
DT	0.7603	0.7586		0.7476
T_2	0.7574	0.7585	0.7559[g]	0.7469

[a]Results using the HF approximations for both electrons and nuclei from Ref. 60.
[b]Results obtained in this work at HF (FCI) level of theory for the nuclei (the electrons).
[c]Values determined from experimental data.[92]
[d]Reference 88.
[e]Reference 89.
[f]Reference 90.
[g]Reference 91.

D_2, DT, and T_2. The nuclear GTFs were obtained using an even-tempered procedure, as outlined in the case of the $[He–H–He]^+$ complex above. Specifically, we employed a 5*spd*/AVQZ basis set for nuclei/electrons. Table V presents the average internuclear distances $\langle R_{n-n} \rangle$ in Å. Experimental,[92] high accurate non-BO results from Adamowicz and collaborators,[88–91] and ENMO results using a HF approach (referred to as HF:HF) for both electrons and nuclei with the APMO code[60] are also displayed. Electronic and nuclear density contours of the HT isotopomer are shown in Figure 7.

By comparing the average $\langle R_{n-n} \rangle$ values for the different isotopes, both experimental and obtained from highly accurate non-BO calculations, it is clear that the heavier the nuclear mass, the shorter the average internuclear distance. This can be understood by considering that the widest amplitude motion, accomplished by the lightest nuclei (i.e., protons), is associated with the highest delocalized nuclear density (see also Figure 7). This trend is well reproduced by both ENMO computations, while the inclusion of the electronic correlation through the FCI approach quantitatively improves the average $\langle R_{n-n} \rangle$ values, as compared to those obtained with highly accurate non-BO methods,[88–91] and estimated from experimental measurements.[92] On the other hand, the incorporation of electronic correlation through BO-based FCI calculations causes an increase of the H–H distance from 0.7326 and 0.7419 Å, indicating that the differences between HF:HF and HF:FCI results with the ENMO approach arise not only from the electronic correlation but also from the corresponding nuclear response. As in the helium dimer case, nuclear relaxation energies reach significant values at short internuclear distances only (see Table III), inducing smaller values of the $\langle R_{n-n} \rangle$ when electronic correlation effects are included. As expected, the shortening of the average $\langle R_{n-n} \rangle$ distances becomes more marked as the isotope mass decreases (see Table V). The isotope dependence of the response to the electronic correlation is also clearly apparent by comparing the electronic densities obtained at CCSD(T) and HF levels of theory (see Figure 7): the differences between CCSD(T) (red lines) and HF (grey lines) density contours are more pronounced around the lightest quantum nucleus, becoming almost indistinguishable at the infinite nuclear limit. This shows

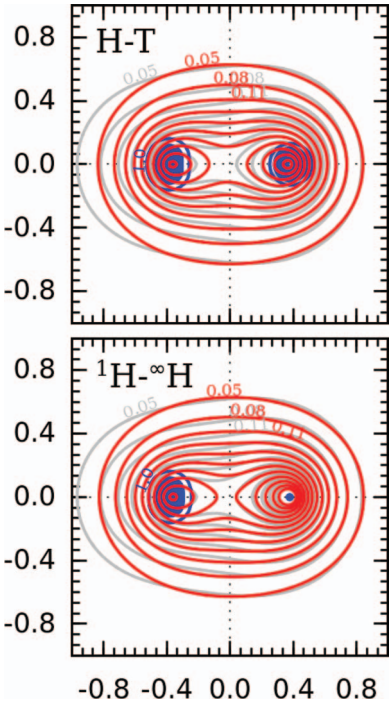

FIG. 7. Contour plots of the electronic (highlighted in red) and nuclear (highlighted in blue) densities on a plane containing the internuclear axis (in Å units). Electronic density distributions obtained at HF level of theory (grey color) have been superimposed. (Upper panel) molecular HT. (Lower panel) H_2 at the infinite nuclear limit for one of the hydrogen nuclei (denoted as $^\infty H_2$). Adjacent contours are separated by 0.03 a.u.

the importance of including the electronic correlation effects in the quantum treatment of the lightest nuclei.

Focusing on the electronic densities shown in Figure 7 for molecular HT, it can be noticed that the electronic cloud around the lightest isotope becomes more dispersed. On a contrary, the electronic charge tends to concentrate more at nuclear-rich regions as the isotope mass increases. This is further clarified in the infinite-nuclear mass limit for one of the hydrogen atoms (see the bottom panel of Figure 7). As discussed above for the helium dimer, this can be explained by comparing bare and dressed *e-n* Coulomb interactions in Figure 2: the bare Coulomb interaction, corresponding to the infinite-nuclear mass limit, is capable of attracting more electronic density into the nucleus position. Naturally, this is reflected in molecular dipole moment μ values. This property has been experimentally determined for heteronuclear HD by Nelson and Tabisz,[93] providing a value in the range 0.8–1.0 mD. This value is overestimated by a factor of 28 by our HF:FCI calculations which is similar to factor of 30 obtained from earlier HF:HF calculations.[60] As extensively discussed by Ishimoto *et al.*,[43] the inclusion of electron-nuclear correlation is very important to obtain μ values in good agreement with the experimental measurements. In fact, by resorting to the FCI *fully variational* MO method (see Sec. I), they provided a value of the HD dipole moment of 0.85 mD in excellent agreement with the experimental measurements. Similar to the $[He-H-He]^+$ system, electron-nuclear correlation effects result in more delocalized nuclear density distributions. Therefore, the electronic density becomes even more

dispersed floating out from the classical nuclei positions and providing smaller μ values. Accurate results have been also given by Adamowicz and collaborators in Ref. 17 (for example, $\mu = 0.83$ mD for HD). The nuclear mass dependence of these values is already qualitatively captured in our calculations (μ(HT) > μ(HD) > μ(DT)). However, the poor quantitative agreement for the μ values indicates the importance of adopting higher levels of theory to describe this property. As already mentioned, the separation of the center-of-mass motion can be emulated by freezing the position of one nucleus and replacing the mass of the second nucleus by the molecular reduced mass. This numerical test has been carried out for the HD molecule resulting in the lowering of the nuclear kinetic energy by more than 0.02 a.u. Still, the electron-nuclear correlation must be included to provide more accurate values of diatomic non-BO energies. Moreover, it should be stressed that at present the APMO-MOLPRO interface allows to handle only maximum spin states for the nuclei with non-zero spin. Therefore, our results on H_2 correspond to the *ortho*-H_2 spin isomer. The experimental measurements, however, usually involve a mixture of *ortho*- and *para*-H_2 spin isomers.

IV. CONCLUDING REMARKS AND FUTURE PROSPECTS

We report the application of the APMO-MOLPRO interface to three model systems. This computational implementation allows to incorporate nuclear quantum effects at HF level into highly correlated electronic structure calculations carried out with the MOLPRO package.[69] On the other hand, the APMO-MOLPRO interface extends the capabilities of the APMO code by allowing not only to include the electronic correlation but also an efficient optimization of either the nuclear basis set or the molecular geometry. The APMO-MOLPRO implementation is designed in a way that MOLPRO calculations can be performed with an internal call to the APMO code.

To model a weakly interacting system, we have chosen an effective potential for the dimer $^4He_2$ with the bare electronic-nuclear Coulomb interaction replaced by a dressed interaction, substituting the point charges of classical nuclei by corresponding finite nuclear charge distributions. Our results indicate that the requirements for the electronic basis set size and the many-particle correlation treatment become less demanding when electron and nuclei are described simultaneously. This result is interpreted on the basis of *ab initio* calculations using *floating* electronic orbitals, and the relaxation of the cusp conditions upon replacing the bare Coulomb interaction by that obtained after including finite-mass effects. In a future, the distributed Gaussian functions method of Hamilton and Light[82] could be adapted to deal with vibrational ground and excited states of weakly bound systems in ENMO-type implementations.

As a second test case, the APMO-MOLPRO interface has been applied to the $[He–H–He]^+$ molecule and its isotopomers. As reported in previous ENMO studies on the same system,[61] the de-localization degree of the nuclear density is found to be strongly correlated with the nuclear mass. Thus, proton density is isotropic and much more delocalized compared to its deuteron and tritium counterparts. Similarly, the occurrence of anisotropic density shapes for deuteron and tritium is explained on the basis of their lower zero point energies and thus closer following the classical potential energy surface. On the other hand, the comparison with NEO-XCHF2 results from Hammes-Schiffer and collaborators[49] highlights the importance of the electron-nuclear correlation resulting in more delocalized nuclear densities.

A third application considers molecular hydrogen and isotopomers. Although our results are consistent with previous works using the ENMO approach at either lower or higher levels of theory, they clearly show that the inclusion of nuclear-electron correlation effects is necessary. The comparison of HF electronic densities with those calculated at CCSD(T) level of theory for the different isotopomers highlights the importance of including electronic correlation effects in the quantum treatment of the lightest nuclei. Numerical tests, including the separation of the nuclear mass motion, lead to significant total energy differences.

As a future extension, the trans-correlated Hamiltonian approach[84] can be implemented as it can be formulated to include inter-particle short-range correlation through Hartree-like equations. On the other hand, to describe excited states for the nuclear wave-function, the simple version of the frozen local hole approximation (FLHA) developed by Pahl and Birkenheuer[94] could be used, with electrons replaced by protons. This FLHA method has been already implemented in the development version of the MOLPRO package.[95] Since proton density distributions are rather localized as compared with electronic densities, the most obvious advantage of such approach is that only a few self-consistent field (SCF) and non-orthogonal CI calculations would be probably necessary.

Altogether, our results suggest that the simultaneous treatment of the lightest nuclei and electrons in weakly bound systems could provide better convergence with respect to the level of theory. However, it is very important to address the problems associated with: (1) the non-separation of the center-of-mass; (2) the insufficient flexibility of the nuclear basis set; and (3) the non-inclusion of the electron-nuclear correlation before the ENMO-type implementation can be used to accurately represent the molecular energy levels. These enhancements along with the implementation of *h*- and *i*-type functions for the electrons will allow us to perform more rigorous analysis of the electronic and total energies convergence with respect to the basis set size. Our numerical tests for diatomic molecules indicate that the ENMO approach could be reformulated in terms of a translationally invariant molecular Hamiltonian (see, for example, Ref. 96). To account for wide amplitude intramolecular quantum modes, the implementation of the distributed Gaussian method that has been successfully applied to post-BO studies of $^4He_2$ and $^4He_3$,[83] is envisaged. The most appealing advantage of this method is that it preserves the analogies with standard electronic structure implementations through the addition of mid-bond functions, enabling an extension to account also for excited vibrational states. Work along these lines is currently in progress.

ACKNOWLEDGMENTS

We thank Claude Leforestier and Hendrik J. Monkhorst for very useful discussions and suggestions. This work has been performed under Grant Nos. FIS2011-29596-C02-01 from MEC, Spain and a CSIC-COLCIENCIAS joint project (Ref. P2008CO1). The support of COST Action CM1002 "Convergent Distributed Environment for Computational Spectroscopy" (CODECS) is also acknowledged. N.F.A. has been supported by a predoctoral JAE fellowship from the CSIC. The calculations were performed at the Cesga Super-Computer Center (Galicia) and the Computer Centers at the IFF (CSIC) and the Centro Técnico de Informática (CTI, CSIC).

[1] S. Grebenev, J. P. Toennies, and A. F. Vilesov, Science **279**, 2083 (1998).
[2] P. Jungwirth and A. I. Krylov, J. Chem. Phys. **115**, 10214 (2001).
[3] D. López-Durán, M. P. de Lara-Castells, G. Delgado-Barrio, P. Villarreal, C. Di Paola, F. A. Gianturco, and J. Jellinek, Phys. Rev. Lett. **93**, 053401 (2004).
[4] M. P. de Lara-Castells, D. López-Durán, G. Delgado-Barrio, P. Villarreal, C. Di Paola, F. A. Gianturco, and J. Jellinek, Phys. Rev. A **71**, 033203 (2005).
[5] M. P. de Lara-Castells, G. Delgado-Barrio, P. Villarreal, and A. O. Mitrushchenkov, J. Chem. Phys. **125**, 221101 (2006).
[6] M. P. de Lara-Castells, P. Villareal, G. Delgado-Barrio, and A. O. Mitrushchenkov, J. Chem. Phys. **131**, 194101 (2009).
[7] M. P. de Lara-Castells and A. O. Mitrushchenkov, J. Phys. Chem. Lett. **2**, 2145 (2011).
[8] N. F. Aguirre, P. Villarreal, G. Delgado-Barrio, A. O. Mitrushchenkov, and M. P. de Lara-Castells, Chem. Phys. Lett. **555**, 12 (2013).
[9] I. L. Thomas, Phys. Rev. **185**, 90 (1969).
[10] I. L. Thomas, Chem. Phys. Lett. **3**, 705 (1969).
[11] I. L. Thomas and H. W. Joy, Phys. Rev. A **2**, 1200 (1970).
[12] I. L. Thomas, Phys. Rev. A **3**, 565 (1971).
[13] D. M. Bishop, Mol. Phys. **28**, 1397 (1974).
[14] D. M. Bishop and L. M. Cheung, Phys. Rev. A **16**, 640 (1977).
[15] H. J. Monkhorst, Phys. Rev. A **36**, 1544 (1987).
[16] L. Wolniewicz, J. Chem. Phys. **99**, 1851 (1993).
[17] M. Cafiero, S. Bubin, and L. Adamowicz, Phys. Chem. Chem. Phys. **5**, 1491 (2003).
[18] S. Bubin, M. Cafiero, and L. Adamowicz, Adv. Chem. Phys. **131**, 377 (2005).
[19] S. Bubin, M. Pavanello, W. C. Tung, K. L. Sharkey, and L. Adamowicz, Chem. Rev. **113**, 36 (2013).
[20] E. Mátyus and M. Reiher, J. Chem. Phys. **137**, 024104 (2012).
[21] A. D. Bochevarov, E. F. Valeev, and C. D. Sherrill, Mol. Phys. **102**, 111 (2004).
[22] M. Goli and S. Shahbazian, Theor. Chem. Acc. **131**, 1208 (2012).
[23] M. Tachikawa, K. Mori, H. Nakai, and K. Iguchi, Chem. Phys. Lett. **290**, 437 (1998).
[24] H. Nakai, Int. J. Quantum Chem. **107**, 2849 (2007).
[25] H. Nakai, K. Sodeyama, and M. Hoshino, Chem. Phys. Lett. **345**, 118 (2001).
[26] H. Nakai, Int. J. Quantum Chem. **86**, 511 (2002).
[27] H. Nakai and K. Sodeyama, J. Chem. Phys. **118**, 1119 (2003).
[28] H. Nakai, M. Hoshino, K. Miyamoto, and S. Hyodo, J. Chem. Phys. **122**, 164101 (2005).
[29] H. Nakai, M. Hoschino, K. Miyamoto, and S.-a. Hyodo, J. Chem. Phys. **123**, 237102 (2005).
[30] M. Hoshino and H. Nakai, J. Chem. Phys. **124**, 194110 (2006).
[31] B. Sutcliffe, J. Chem. Phys. **123**, 237101 (2005).
[32] M. Hoshino, H. Nishizawa, and H. Nakai, J. Chem. Phys. **135**, 024111 (2011).
[33] H. Nishizawa, M. Hoshino, Y. Imamura, and H. Nakai, Chem. Phys. Lett. **521**, 142 (2012).
[34] H. Nishizawa, Y. Imamura, Y. Ikabata, and H. Nakai, Chem. Phys. Lett. **533**, 100 (2012).
[35] T. Ishimoto, M. Tachikawa, and U. Nagashima, Int. J. Quantum Chem. **109**, 2677 (2009).
[36] T. Udagawa and M. Tachikawa, *Multi-Component Molecular Orbital Theory* (Nova Science Publishers, New York, 2009).
[37] M. Tachikawa and K. Osamura, Theor. Chem. Acc. **104**, 29 (2000).
[38] M. Tachikawa, K. Mori, K. Suzuki, and K. Iguchi, Int. J. Quantum Chem. **70**, 491 (1998).
[39] M. Tachikawa, K. Taneda, and K. Mori, Int. J. Quantum Chem. **75**, 497 (1999).
[40] M. Tachikawa, Mol. Phys. **100**, 881 (2002).
[41] M. Tachikawa, Chem. Phys. Lett. **360**, 494 (2002).
[42] T. Ishimoto, M. Tachikawa, M. Yamauchi, H. Kitagawa, H. Tokiwa, and U. Nagashima, Chem. Phys. Lett. **372**, 503 (2003).
[43] T. Ishimoto, M. Tachikawa, and U. Nagashima, J. Chem. Phys. **128**, 164118 (2008).
[44] S. P. Webb, T. Iordanov, and S. Hammes-Schiffer, J. Chem. Phys. **117**, 4106 (2002).
[45] M. W. Schmidt, K. K. Baldrige, J. A. Boatz, S. T. Elbert, M. S. Gordon, J. H. Jensen, S. Koseki, N. Matsunaga, K. A. Nguyen, S. J. Su, T. L. Windus, M. Dupuis, and J. A. Montgomery, J. Comput. Chem. **14**, 1347 (1993).
[46] T. Iordanov and S. Hammes-Schiffer, J. Chem. Phys. **118**, 9489 (2003).
[47] A. Reyes, M. V. Pak, and S. Hammes-Schiffer, J. Chem. Phys. **123**, 064104 (2005).
[48] C. Swalina, M. V. Pak, A. Chakraborty, and S. Hammes-Schiffer, J. Phys. Chem. A **110**, 9983 (2006).
[49] C. Ko, M. V. Pak, C. Swalina, and S. Hammes-Schiffer, J. Chem. Phys. **135**, 054106 (2011).
[50] J. H. Skone, M. V. Pak, and S. Hammes-Schiffer, J. Chem. Phys. **123**, 134108 (2005).
[51] C. Swalina, M. V. Pak, and S. Hammes-Schiffer, Chem. Phys. Lett. **404**, 394 (2005).
[52] J. F. Capitani, R. F. Nalewajski, and R. G. Parr, J. Chem. Phys. **76**, 568 (1982).
[53] Y. Shigeta, H. Takahashi, S. Yamanaka, M. Mitani, H. Nagao, and K. Yamaguchi, Int. J. Quantum Chem. **70**, 659 (1998).
[54] T. Kreibich and E. K. U. Gross, Phys. Rev. Lett. **86**, 2984 (2001).
[55] Y. Imamura, H. Kiryu, and H. Nakai, J. Comput. Chem. **29**, 735 (2008).
[56] Y. Imamura, Y. Tsukamoto, H. Kiryu, and H. Nakai, Bull. Chem. Soc. Jpn. **82**, 1133 (2009).
[57] M. V. Pak, A. Chakraborty, and S. Hammes-Schiffer, J. Phys. Chem. A **111**, 4522 (2007).
[58] T. Udagawa and M. Tachikawa, J. Chem. Phys. **125**, 244105 (2006).
[59] R. Colle and O. Salvetti, Theor. Chem. Acta **37**, 329 (1975).
[60] S. A. González, N. F. Aguirre, and A. Reyes, Int. J. Quantum Chem. **108**, 1742 (2008).
[61] S. A. González and A. Reyes, Int. J. Quantum Chem. **110**, 689 (2010).
[62] D. V. Moreno, S. A. González, and A. Reyes, J. Phys. Chem. A **114**, 9231 (2010).
[63] D. V. Moreno, S. A. González, and A. Reyes, J. Chem. Phys. **134**, 024115 (2011).
[64] F. Moncada, S. A. González, and A. Reyes, Mol. Phys. **108**, 1545 (2010).
[65] F. Moncada, D. Cruz, and A. Reyes, Chem. Phys. Lett. **539**, 209 (2012).
[66] R. Flores-Moreno, V. G. Zakrzewski, and J. V. Ortiz, J. Chem. Phys. **127**, 134106 (2007).
[67] R. Flores-Moreno, S. A. González, N. F. Aguirre, E. F. Posada, J. Romero, F. Moncada, G. Merino, and A. Reyes, LOWDIN: A general code for the treatment of any particle, 2012, see https://sites.google.com/site/lowdinproject/home.
[68] J. Romero, E. F. Posada, R. Flores-Moreno, and A. Reyes, J. Chem. Phys. **137**, 074105 (2012).
[69] H. J. Werner, P. J. Knowles, R. Lindh, F. R. Manby, M. Schütz *et al.*, MOLPRO, version 2009.1, a package of *ab initio* programs, 2009, see http://www.molpro.net.
[70] K. Patkowski, J. Chem. Phys. **137**, 034103 (2012).
[71] D. E. Woon and T. H. Dunning, Jr., J. Chem. Phys. **100**, 2975 (1994).
[72] T. van Mourik, A. K. Wilson, and T. H. Dunning, Jr., Mol. Phys. **96**, 529 (1999).
[73] S. F. Boys and F. Bernardi, Mol. Phys. **19**, 553 (1970).
[74] W. Cencek, M. Przybytek, J. Komasa, J. B. Mehl, B. Jeziorski, and K. Szalewicz, J. Chem. Phys. **136**, 224303 (2012).
[75] K. Taneda and K. Mori, Chem. Phys. Lett. **298**, 293 (1998).
[76] S. Y. Leu and C. Y. Mou, J. Chem. Phys. **101**, 5910 (1994).
[77] M. P. de Lara-Castells, N. F. Aguirre, and A. O. Mitrushchenkov, Chem. Phys. **399**, 272 (2012).
[78] T. Kato, Commun. Pure Appl. Math. **10**, 151 (1957).

[79]Y. Nakatsuka, T. Nakajima, and K. Hirao, J. Chem. Phys. **132**, 174108 (2010).
[80]N. C. Handy, Y. Yamaguchi, and H. F. Schaefer III, J. Chem. Phys. **84**, 4481 (1986).
[81]M. P. de Lara-Castells, N. F. Aguirre, P. Villarreal, G. Delgado-Barrio, and A. O. Mitrushchenkov, J. Chem. Phys. **132**, 194313 (2010).
[82]I. P. Hamilton and J. C. Light, J. Chem. Phys. **84**, 306 (1986).
[83]T. González-Lezana, J. Rubayo-Soneira, S. Mirét-Artés, F. A. Gianturco, G. Delgado-Barrio, and P. Villarreal, Phys. Rev. Lett. **82**, 1648 (1999).
[84]H. Luo, J. Chem. Phys. **133**, 154109 (2010).
[85]I. Baccarelli, F. Gianturco, and F. Schneider, J. Phys. Chem. A **101**, 6054 (1997).
[86]J. J. Liang, C. L. Yang, L. Z. Wang, and Q. G. Zhang, J. Chem. Phys. **136**, 094307 (2012).
[87]A. N. Panda and N. Sathyamurthy, J. Phys. Chem. A **107**, 7125 (2003).
[88]S. Bubin, F. Leonarski, M. Stanke, and L. Adamowicz, Chem. Phys. Lett. **477**, 12 (2009).
[89]M. Stanke, S. Bubin, M. Molski, and L. Adamowicz, Phys. Rev. A **79**, 032507 (2009).
[90]S. Bubin, M. Stanke, and L. Adamowicz, J. Chem. Phys. **135**, 074110 (2011).
[91]S. Bubin, M. Stanke, M. Molski, and L. Adamowicz, Chem. Phys. Lett. **494**, 21 (2010).
[92]K. P. Huber and G. Herzberg, *Molecular Spectra Molecular Structure, Constants of Diatomic Molecules* (Van Nostrand Reinhold, New York, 1979).
[93]J. B. Nelson and G. C. Tabisz, Phys. Rev. A **28**, 2157 (1983).
[94]E. Pahl and U. Birkenheuer, J. Chem. Phys. **124**, 214101 (2006).
[95]M. P. de Lara-Castells and A. O. Mitrushchenkov, J. Phys. Chem. C **115**, 17540 (2011).
[96]B. T. Sutcliffe and R. G. Woolley, J. Chem. Phys. **137**, 22A544 (2012).